LOW-COST PASSIVE UHF RFID TAGS ON PAPER SUBSTRATES

A Thesis
Submitted to the Graduate Faculty
of the
North Dakota State University
of Agriculture and Applied Science

By

Sayeed Zebaul Haque Sajal

In Partial Fulfillment
for the Degree of
MASTER OF SCIENCE

Major Department:
Electrical and Computer Engineering

May 2014

Fargo, North Dakota

North Dakota State University
Graduate School

Title

Low-Cost Passive UHF RFID Tags on Paper Substrates

By

Sayeed Zebaul Haque Sajal

The Supervisory Committee certifies that this ***disquisition*** complies with North Dakota State University's regulations and meets the accepted standards for the degree of

MASTER OF SCIENCE

SUPERVISORY COMMITTEE:

Dr. Benjamin D. Braaten
Chair

Dr. Ivan T. Lima

Dr. David A. Rogers

Dr. Val R. Marinov

Approved:

7/7/2014
Date

Dr. Scott Smith
Department Chair

ABSTRACT

To reduce the significant cost in the widespread deployment of UHF radio frequency identification (RFID) systems, an UHF RFID tag design is presented on paper substrates. The design is based on meander-line miniaturization techniques and open complementary split ring resonator (OCSRR) elements that reduce required conducting materials by 30%. Another passive UHF RFID tag is designed to sense the moisture based on the antenna's polarization. An inexpensive paper substrate and copper layer are used for flexibility and low-cost. The key characteristic of this design is the sensitivity of the antenna's polarization on the passive RFID tag to the moisture content in the paper substrate. In simulations, the antenna is circularly-polarized when the substrate is dry ($\epsilon_r = 2.38$) and is linearly-polarized when the substrate is wet ($\epsilon_r = 35.35$). It was shown that the expected read-ranges and desired performance could be achieved reducing the over-all cost of the both designs.

ACKNOWLEDGMENTS

Firstly I would like to thank my Almighty Allah for His endless blessings on me.

Secondly I would like to express my sincere thanks to my adviser, Dr. Benjamin D. Braaten for providing immense guidance, strong support, inspiration and supervision throughout my studies and research at North Dakota Sate University.

I am really grateful to Dr. Ivan T. Lima, Dr. David A. Rogers and Dr. Val. R. Marinov to give me inspiration and guidance to achieve my goal.

Finally, I would like to express a special thanks to my family for their support and inspiration.

DEDICATION

To my family.

TABLE OF CONTENTS

LIST OF TABLES

LIST OF FIGURES

LIST OF SYMBOLS

θ ..... angle in spherical co-ordinate system

ϕ ..... angle in spherical co-ordinate system

σ ..... conductivity

ϵ ..... electrical permittivity

ϵ_o ..... free space permittivity

ϵ_r ..... relative permittivity

ξ ..... instantaneous field of plane wave

τ ..... power transmission coefficient

Δ ..... difference

CHAPTER 1. INTRODUCTION

Reducing the cost of passive UHF Radio Frequency Identification (RFID) tags has been of great interest to designers for many years [1]-[2]. This is because simple item level tracking and sensing are the major applications and a long-term goal of passive UHF RFID systems [1]. To track individual items, bar codes have been used successfully for the past several decades [2]. This is because bar codes can be printed for little cost on a paper material and scanned (i.e., read) with a hand-held optical device. Furthermore, outside of the retail industry, bar codes have been applied to 1) increasing safety in medical and clinical systems, 2) storage and shipping of parts in the automotive sector and 3) logistics in the processing and manufacturing industry [2]. In all of these cases the application of a bar code has been cost effective; however, to scan a bar code in many of these settings, a user must be within 25 cm of the item. Because of this small distance, if a UHF RFID system based on far-field communication techniques is deployed for item level tracking, the passive tag on the item will be in the near-field of the reader antenna. This near-field proximity of the tag has led to much research and development on the design of near-field UHF reader antennas [3]-[6] and coil antennas [2] for the passive RFID tags in the UHF and HF bands, respectively.

One of the major limitations facing the widespread deployment of UHF RFID systems is the cost of each individual passive tag. This expense is especially apparent when considering a near-field UHF RFID system because much of the cost associated with the passive tag is the conducting material used to manufacture the antenna and the passive IC. Therefore, the objective of this thesis is to present an antenna design for a passive near-field UHF RFID tag that uses very little conducting material and can be printed on a low-cost paper substrate. Then, as a demonstration, the antenna design will be used to develop a prototype passive RFID tag with a Higgs3 IC, by

Alien Technologies [7], in the 902 - 928 MHz UHF band. Specifically, the performance of the prototype tag will be determined at 920 MHz which is the operating frequency of the prototype tag.

Next, to minimize the cost of a passive UHF RFID moisture sensor, which can sense the wetness remotely, is a big challenge. There are many solutions based on different technologies. In reference to [8] the paper-based semi-passive RFID was used a built-in energy conversion sensor.As this is semi-passive it is not cost-effective because of the power source Some other technology uses the following: passive LC resonating sensor tag [9] where inductive coupling was used between the sensor tag and n interrogator circuit, a plurality of conductor pairs [10] where power device was used and this one was not wireless, RFID tag activation by a fluid [11] where copper (Cu) layer, copper chloride (CuCl)-doped filter paper and a magnesium (Mg) layer was used for paper battery, an RFID transponder comprising sensor element [12], a waste detection system [13], electric voltage difference [14] and hygroscopic polymer [15] for low-cost sensing. The objective of the new technology is to minimize the cost and to increase the ease of use.

In this thesis the cost is reduced by using very inexpensive paper substrates, a Higgs2 IC and copper as a conductive layer. The permittivity of the paper substrate is changed with the addition of moisture [16]. Based on this principle, a new antenna is fabricated where the dipole antenna uses polarization to differentiate whether it is dry or wet. In measurements the antenna actually uses the ratio of the reading distances of the differently oriented antennas to sense the moisture in the paper [17]-[24].

CHAPTER 2. AN INTRODUCTION TO RFID AND THEORY

2.1. Radio Frequency Identification (RFID)

RFID is a popular technology which has an economic impact in many industries. It is a very smart element in remote identification process, and it can also be used for sensing and tracking applications, which is useful and cost effective in many industries.

2.1.1. Classification and standard

The RFID system can be classified depending on the power source[25], operating frequency range according to EPCglobal standard[26] and International Organization of Standardization(ISO) standard[27]. These are shown in details in Table 1, Table 2 and Table 3.

Table 1. Classification of RFID based on power source.

Tag Type	**Passive**	**Semi passive**	**Active**
Power source	Harvesting energy	Battery	Battery
Communication	Response only	Response only	Respond or initiate
Max Range	10 m	>100 m	>100 m
Relative Cost	Least expensive	More expensive	Most expensive
Applications	Proximity cards	Electric toll	Asset, livestock

Table 2. Classification of RFID based on operating frequency range with EPCglobal standard.

Frequency Range	**Frequencies**	**EPCglobal Standard**
Low Frequency (LF)	below 135 kHz	No reference found
High Frequency (HF)	13.56 MHz	EPC class1 HF
Ultra-High Frequency (UHF)	860 MHz-960 MHz	EPC class1 Gen2 UHF

Nowadays, the Electronic Product Code (EPC) class1 Gen2 UHF RFID is most widely used for tracking and sensing purpose. Though the operating frequency range

of this kind of RFID is 860 MHz to 960 MHz, there are specific ranges based on the geographical location of the operation. For example, USA and CANADA (902 MHz - 928 MHz), Europe (865.6 MHz - 867.6 MHz) and Japan (952 MHz - 954 MHz)[28]. So it is very important to know the end-user location for RFID design of a particular application.

Table 3. RFID international standard developed by ISO.

International standard	**Description**
ISO/IEC 18000-1:2008	Definition of parameters
ISO/IEC 18000-2:2009	Air interface below 135 KHz
ISO/IEC 18000-3:2010	Air interface at 13.56 MHz
ISO/IEC 18000-4:2008	Air interface at 2.45 GHz
ISO/IEC 18000-6:2013	Air interface at 860 MHz to 960 MHz
ISO/IEC 18000-7:2009	Air interface at 433 MHz

2.1.2. Advantages and disadvantages

- Advantages of RFID
  - RFID is very fast compared to bar codes. Current second generation tags can read more than 1600 tags/sec[28].
  - The RFID reader does not require a clear line of sight to read the RFID though some obstacles are worse than others.
  - RFID can be read from a longer distance. For example passive RFID can be read to about 5m, semi-passive or active can read from 50m-500m where read-range of bar codes is less than 1 m.
  - The RFID data capacity higher than bar codes.
  - RFID is very robust. They can tolerate high and low temperature, they can be read even when it is bent, dirty or painted.

  - Modern RFID allows users to modify the data on the RFID tag.
  - RFID can be connected to sensors for humidity, temperature, orientation, speed and other environmental information.

- Disadvantages of RFID
  - RFIDs are expensive compared to bar codes.

2.2. Theory

2.2.1. Theory of RFID

An RFID system basically consists of an integrated circuit(IC) and an antenna.The antenna needs to be designed on a defined substrate in such a way that it can match the complex conjugate of the of the IC's input impedance at a particular frequency. The data capacity of the RFID depends on the IC which is attached to the designed antenna. In this RFID design, the conjugate impedance matching technique is explored in detail[29]. Let, the antenna impedance be defined as $Z_A = R_A + \mathrm{j}X_A$ and the IC impedance be defined as $Z_{IC} = R_{IC} + \mathrm{j}X_{IC}$.

For a particular event, it is assumed that the sensitivity (P_{IC}) of the RFID's transponder (the RF power required to turn on the IC and to perform backscattering modulation between the reader and the tag antennas) and the effective power (EIRP_R) transmitted by the reader are constant. Under the hypothesis of polarization matching between the reader and RFID antennas, the maximum activation distance of the RFID along the (θ,ϕ) direction is given by

$$d_{max}(\theta,\phi) = \frac{c}{4\pi f}\sqrt{\frac{EIRP_R\tau G_{IC}(\theta,\phi)}{P_{IC}}} \tag{2.1}$$

where $G_{IC}(\theta,\phi)$ is the IC gain and τ is written as :

$$\tau = \frac{4R_{IC}R_A}{|Z_{IC} + Z_A|^2} \leq 1. \tag{2.2}$$

τ is the power transmission coefficient which indicates the mismatch between the antenna impedance and IC impedance. As the transponder includes an energy-storage stage, its input reactance is strongly capacitive. The IC impedance depends on the input power. Most of the available RFID ICs in the UHF band exhibit capacitive input reactance. So to match the conjugate of the IC's capacitive reactance the antenna should be inductive. Beyond d_{max} the power collected by the RFID decreases below the IC sensitivity, and, ultimately, the RFID tag becomes unreachable. Thus, utilizing the conjugate matching technique a maximum read-range for the RFID tag can be achieved.

2.2.2. Polarization of the antenna

The polarization of a wave can be defined in terms of a wave radiated (transmitted) or received by an antenna in a given direction.[30]. The instantaneous field of a plane wave traveling in the negative Z direction can be written as

$$\xi(z;t) = \xi_x(z;t)\hat{x} + \xi_y(z;t)\hat{y}. \tag{2.3}$$

The instantaneous components are related to their components:

$$\xi_x(z;t) = E_{xo}\cos(\omega t + kz + \phi_x) \tag{2.4}$$

$$\xi_y(z;t) = E_{yo}\cos(\omega t + kz + \phi_y) \tag{2.5}$$

where,k is the wave number; ϕ_x and ϕ_y are the time-phase differences of the x and y components; E_{xo} and E_{yo} are the maximum magnitudes of the x and y components.

Polarization is a very important factor in the design of an antenna. Polarization can be classified in three types based on the conditions stated below.

- Linear polarization: Linear polarization can be achieved only when $E_{xo} \neq E_{yo}$ and $\Delta\phi = \phi_y$ - ϕ_x = nπ where, n = 0,1,2,3,....

- Circular polarization: Circular polarization can be achieved only when $E_{xo} = E_{yo}$ and $\Delta\phi = \phi_y$ - $\phi_x = \pm(\frac{1}{2} + 2n)\pi$ where, n = 0,1,2,3,....

- Elliptical polarization: Elliptical polarization can be achieved only when $E_{xo} \neq E_{yo}$ and $\Delta\phi = \phi_y$ - $\phi_x = \pm(\frac{1}{2} + 2n)\pi$ where, n = 0,1,2,3,....

  Finally for elliptical polarization, the ratio of the major and minor axis of the ellipse is defined as AR = $\frac{MajorAxis}{MinorAxis}$ where AR is the axial ratio.

CHAPTER 3. A LOW-COST COMPACT ANTENNA DESIGN ON A PAPER SUBSTRATE FOR NEAR-FIELD PASSIVE UHF RFID TAGS.

3.1. Introduction

[1]A low-cost UHF compact antenna design with a Higgs3 IC is presented in this chapter. The layout of the proposed antenna is shown in Figure 1(a). This antenna design is based on the Open Complementary Split Ring Resonator (OCSRR) element presented in [31]. However, to reduce the conducting material and the overall size of the antenna, the Meander Open Complementary Split Ring Resonator (MOCSRR) element presented in [32]-[33] was adopted. More specifically, the new element design shown in Figure 1(b) was developed in this work. This design uses a meander-line approach to reduce the overall size of the element and conducting regions with low current densities were removed to reduce the cost. This new element is denoted as the R-MOCSRR element where the letter R was added to emphasize the reduced-material benefit. Finally, to reduce the cost further, the antenna will be printed on a low-cost paper substrate [34].

By reducing the cost of passive UHF RFID tags, new item level tracking systems with tags that have the capability of storing product specific information could be developed, which may not be possible with current bar code systems. This could also include the development of new passive RFID ICs with sensors for measuring temperature, orientation, pressure, moisture, vibrations, speed, acceleration, directions as well as other important store information on the history of the product.

[1]The materials in this chapter was co-authored by Sayeed Z. Sajal. He was involved with this work and he was responsible for the fabrication, simulation and measuring the prototype. Sayeed Z. Sajal was the one of the key developers of this work and some of his ideas was implemented in this work. He also drafted and revised all versions of this chapter.

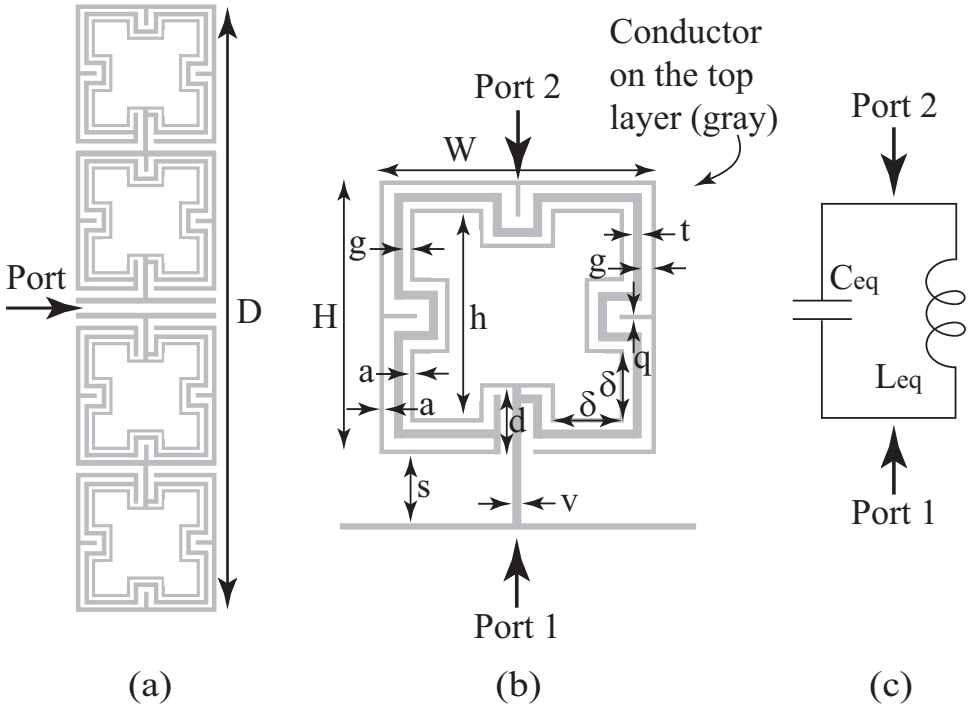

Figure 1. (a) Layout of the proposed antenna consisting of interconnected R-MOCSRR elements with reduced conducting material; (b) configuration of the R-MOCSRR element and (c) equivalent circuit of the R-MOCSRR element.

3.2. Analysis of the R-MOCSRR Element

3.2.1. Benefits of the R-MOCSRR element

The input reactance of a dipole antenna is capacitive below the resonant frequency; therefore, one method to reduce the overall size of a dipole is to introduce inductive loading along the length of each dipole arm to cancel some of the input capacitance. The equivalent circuit of the R-MOCSRR element is shown in Figure 1(c) and consists of a parallel connected capacitance and inductance. The value of L_{eq} represents the loop inductance introduced by the meander-line connected between ports 1 and 2, and C_{eq} represents the capacitance between the meander-line and the reference planes separated by the gap g. By interconnecting the R-MOCSRR elements in the manner shown in Figure 1(a) and designing the R-MOCSRR element to have a resonant frequency above the 902 - 928 MHz UHF band, inductive loading of the dipole can be achieved for antenna miniaturization.

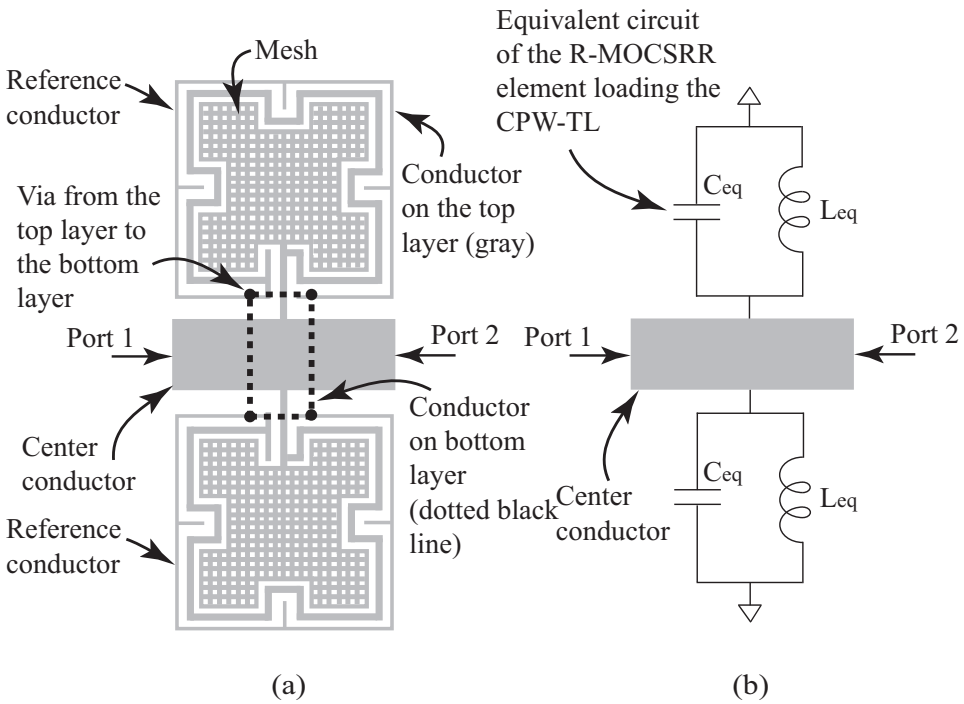

Figure 2. (a) Illustration of the CPW-TL being loaded by the R-MOCSRR element and (b) equivalent circuit of the R-MOCSRR element loading the CPW-TL.

3.2.2. Equivalent circuit of a R-MOCSRR element

To extract the equivalent circuit of the R-MOCSRR element, the coplanar waveguide (CPW) transmission line (TL) shown in Figure 2(a) was first modeled in the commercial software Momentum [35]. The CPW-TL consists of two R-MOCSRR elements connected between the center conductor and the reference planes, and is printed on the top conducting layer. Vias are used to connect the reference planes on the top layer to conductors on the bottom layer. This provides the same reference for both resonators. This configuration then loads the center conductor with the R-MOCSRR elements and results in the equivalent circuit shown in Figure 2(b). By simulating the S-parameters of the layout in Figure 2(a) in Momentum, the resonant frequency f_{oe} of the R-MOCSRR elements can be determined. Then, f_{oe} can be used to extract the equivalent circuit values C_{eq} and L_{eq} in Figure 2(b) using the iterative process summarized in [31]. The accuracy of this extraction method has

been validated in [32]-[33] with a comparison between Momentum simulations and measurements. Furthermore, it was assumed that the overall element sizes W and H in Figure 1(b) were electrically small enough for accurate modelling by the equivalent circuit in Figure 1(c) in the band around the resonant frequency of the R-MOCSRR element.

Table 4. Extracted equivalent circuit values for the three different mesh densities.

Mesh density	L_{eq}	C_{eq}	Z_{eq} at 920 MHz
100% (filled)	8.2 nH	1.1 pF	+j67.1 Ω
50%	8.2 nH	1.1 pF	+j67.1 Ω
0% (not filled)	5.2 nH	1.6 pF	+j41.2 Ω

Table 5. Extracted resonant frequency values for the three different mesh densities.

Mesh density	$f_{oe,ads}$	$f_{oe,cir}$
100% (filled)	1.75 GHz	1.67 GHz
50%	1.75 GHz	1.67 GHz
0% (not filled)	1.77 GHz	1.74 GHz

3.2.3. Characteristics of the R-MOCSRR element

Next, the equivalent circuit of the R-MOCSRR element in Figure 2(a) was extracted for three different configurations on a 55 μm thick paper substrate with ε_r = 2.38. One configuration had all of the copper removed from the middle conducting plane with the exception of the outline (as shown in Figure 1(b)), one configuration had a mesh defined over the middle conducing plane (as shown in Figure 2(a)) and the last configuration had no conducting material removed from the middle conducting plane. The conductor widths were 0.21 mm and the spacing between these conductors of the mesh were 0.25 mm. These configurations were done to explore

the characteristics of the R-MOCSRR element for different quantities of conducting material. The extracted circuit values and associated resonant frequencies of the R-MOCSRR elements f_{oe} are summarized in Tables 4 and 5, respectively. Also, the S_{11} result for the R-MOCSRR element without a mesh density (as shown Figure 1(b)) is shown in Figure 3 to illustrate how well the equivalent circuit in Figure 2(b) models the CPW-loadedl TL in Figure 2(a). Notice that f_{oe} is above the operating frequency of the tag, which allows the designer to introduce inductance along the length of the antenna on the tag.

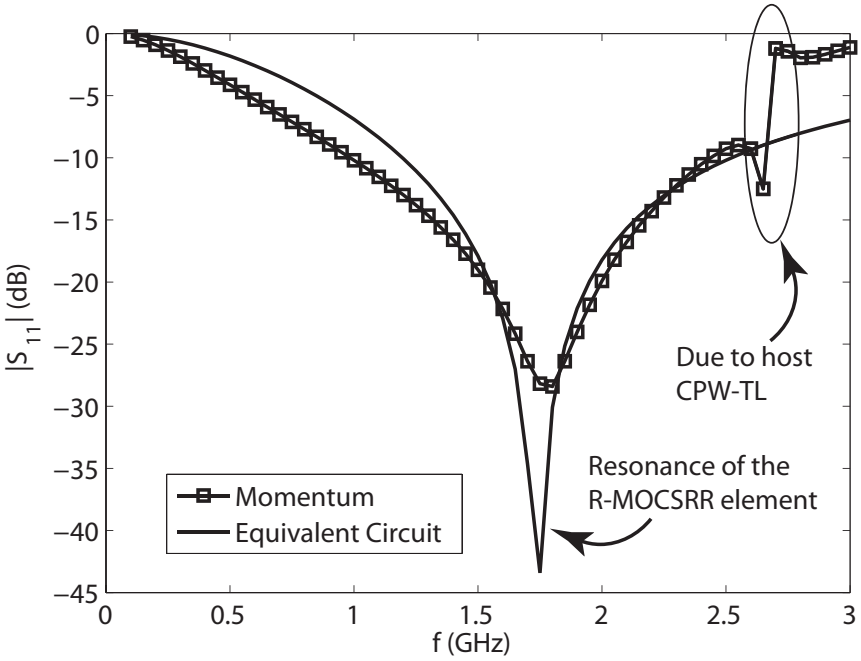

Figure 3. S_{11} values of the R-MOCSRR unit cell with the mesh removed simulated in Momentum and modeled using the equivalent circuit of R-MOCSRR.

For this design, an additional requirement of minimizing the conducting material is present. The results in Tables 4 and 5 show that the inductance is only reduced slightly and the resonant frequency of the R-MOCSRR element still remains above the UHF operating band when the conducting material from the middle conducting plane is removed.

Furthermore, the impedance introduced by the R-MOCSRR element is computed at 920 MHz in the last column of Table 4 and in all cases the reactance is inductive, indicating that the element can be used to inductively load an antenna and is suitable for designing miniaturized antennas for near-field UHF RFID applications.

3.3. The R-MOCSRR Near-field UHF RFID Tag Antenna

3.3.1. Prototype tag design requirements

For near-field UHF RFID applications, a long read-range is not desired and the main focus is to reduce the overall size and minimize the conductive material used to manufacture the antenna. In fact, a long read-range with this antenna design is not desirable in some cases. For instance, security can be enhanced with tags that have a low read-range. Also, when considering item level tracking in a crowded RFID environment, if the read-range of a tag is comparable to commercially available RFID tags of 5-10 m, an item may be scanned by two different readers. One reader may be an unwanted reader using far-field techniques, and the intended reader may be using near-field techniques. Therefore, to reduce the read-range of a tag, mismatching at the port between the antenna and the tag is used. This can be used to avoid unwanted reads from powerful far-field readers. Then again, the main focus of this work is to minimize size and cost, and further efforts could be taken to extend the read-range (if desired) with better matching.

3.3.2. Designing and manufacturing the prototype tag

The antenna design in Figure 1(a) was simulated in Momentum on a 55 μm thick paper substrate. In order to minimize the material cost, the R-MOCSRR element shown in Figure 1(b) without the mesh was chosen. The results in Tables 4 and 5 show that inductive loading can still be achieved with an element that uses 30% less material. The antennas were printed by standard screen printing techniques using a Speedline Technologies [36] SPM/B model screen printer and a stainless steel (230-

0.0014) screen with a 0.0005" emulsion thickness and a 45 degree wire angle. The antenna was screen printed on a Strathmore Marker 500 series cotton based 55 μm thick paper substrate with a measured relative permittivity of $\varepsilon_r = 2.38$. The silver-filled conductive paste used was Acheson Electrodag PF-050 [37] which was designed for printing on flexible substrates such as paper. The screens and the parameters used for printing were selected based on the recommendation by the material manufacturer and optimized in prior projects. Sintering of the ink was done at 150 degrees C for 5 minutes in an Espec convection oven. The printed prototype antenna is shown in Figure 4, and the paper substrates showed no sign of temperature exposure. The dimensions of the antenna made of inexpensive paper are also shown in the caption of Figure 4.

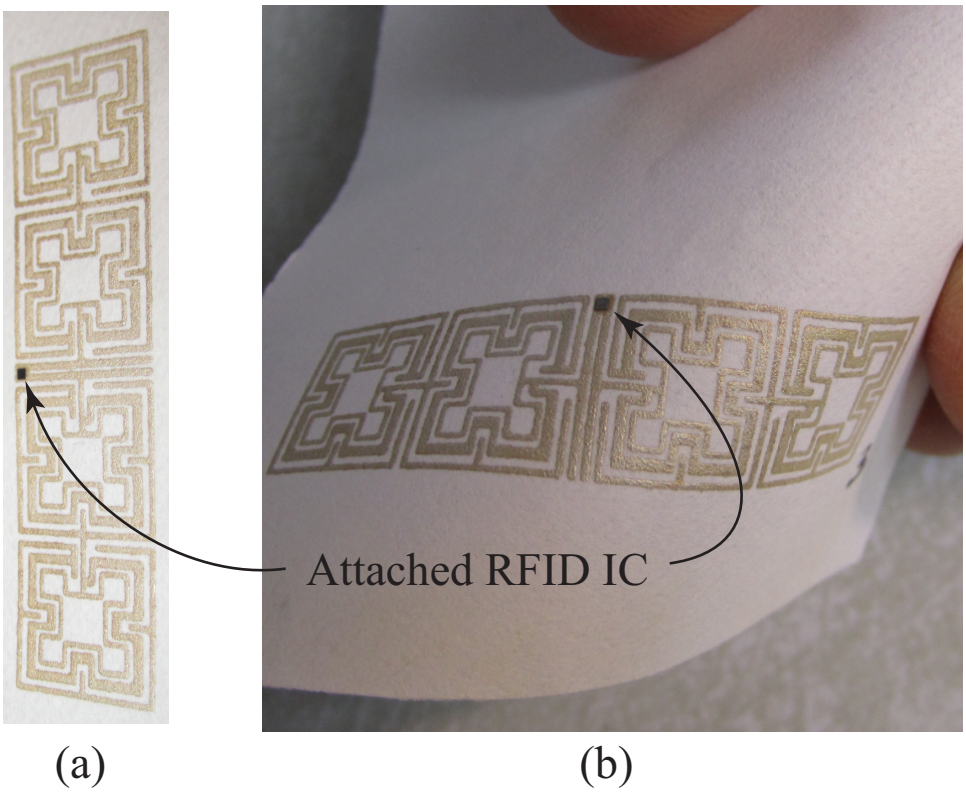

Figure 4. (a) Picture of the screen printed prototype antenna and (b) a picture showing the flexibility of the prototype antenna (a = 0.3 mm, d = 1.3 mm, g = 0.5 mm, h = 5.5 mm, q = 0.3 mm, s = 0.4 mm, t = 0.6 mm, v = 0.3 mm, δ = 2.1 mm, D = 40.5 mm, H = 9.4 mm and W = 10.5 mm).

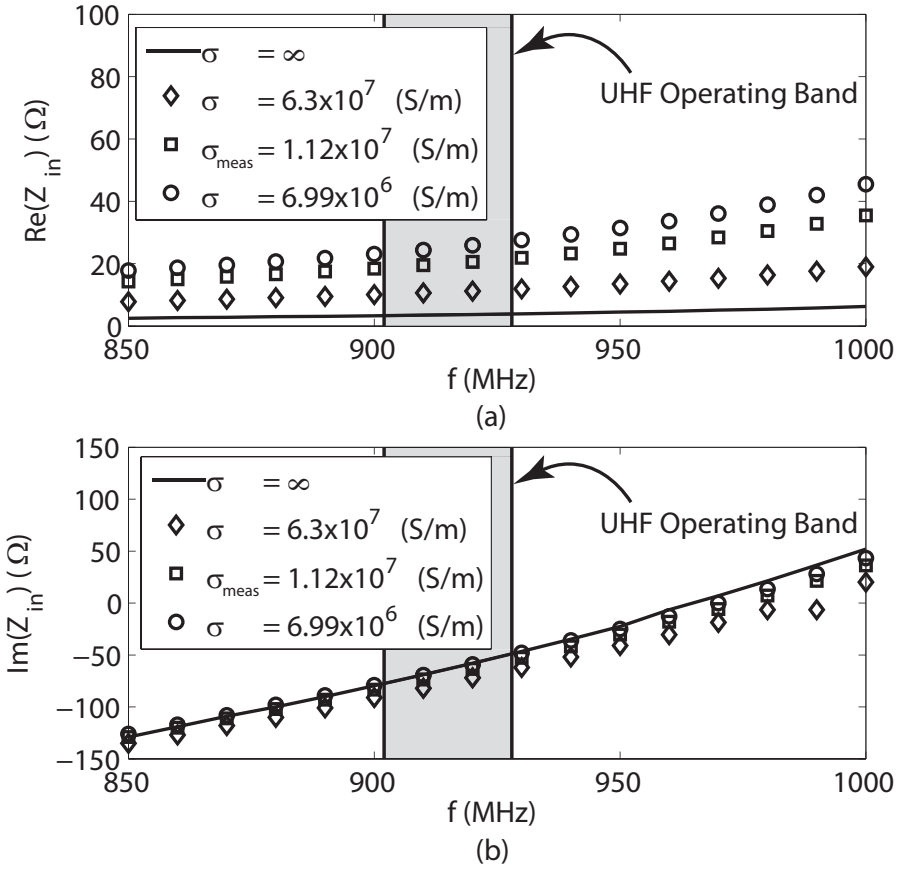

Figure 5. (a) Simulated input resistance of the prototype near-field UHF RFID tag on the paper substrate for various values of conductivity and (b) simulated input reactance of the prototype near-field UHF RFID tag on the paper substrate for various values of conductivity.

The R-MOCSRR unit cell evaluated in Figure 1(a) without the mesh density was used for the antenna design, and the S-parameter values of this unit-cell are shown in Figure 3. Furthermore, the thickness of the screen printed traces of the antenna was measured to be 9.3 μm. Then, using a DC probe, the conductivity was measured to be $\sigma_{meas} = 1.12 \times 10^7$ S/m, which is less than the conductivity of bulk silver. However, this is anticipated because of the particle nature of the ink. Next, the input impedance and gain values of the antenna were determined in ADS for various values of conductivity σ. The computed input impedance values are shown in Figure 5 and the simulated gain of the prototype antenna at 920 MHz was determined to

be G_s = -6.9 dBi for σ = 6.99× 10^6 (S/m), G_s = -5.9 dBi for σ_{meas} = 1.12× 10^7 (S/m), G_s = -3.5 dBi for σ = 6.3× 10^7 (S/m) and G_s = 1.7 dBi $\sigma = \infty$ (S/m) (i.e., a perfect conductor). Furthermore, the electrical length of a conventional thin-wire dipole with a length equal to the length of the antenna on the prototype design in Figure 4(a) is $L = 0.124\ \lambda$ at 920 MHz; which has a significant input reactance that is capacitive. The results in Figure 5 indicate that the R-MOCSRR elements with the reduced material are inductively loading the new dipole design on the prototype tag. It should also be mentioned that a radiation pattern similar to a dipole antenna was observed.

Table 6. Measured read-range values for the prototype near-field UHF RFID tag at 920 MHz.

Tag number	Read-range (cm)
1	34.2
2	35.5
3	34.2
4	34.2
5	34.2
6	34.2
7	34.2
8	35.5

The passive UHF RFID IC chips used to verify the antenna design in this work were the Higgs3 manufactured by Alien Technologies [7]. The chips were 670 μm/side and mechanically thinned to 65 microns. The Higgs3 RFID chips were manually placed at the port of the antenna shown in Figure 1(a) and attached to the antenna pads using epoxy based Creative Materials [38] EXP 2608-48 anisotropic conductive paste (ACP) with an average particle size of 3 μm. The ACP was applied with a manual dispenser with a needle size of 125 μm. The ACP serves two purposes, namely, electrical contact with the antenna, and it acts as an under fill for the thinned

IC die. To cure the ACP and provide electrical contact the antennas with the chips were placed on a Thermolyne Mirak hot plate at 125 degrees C for 2 min to B-stage cure the epoxy. Final cure was performed (as outlined in the data sheet) on the same hot plate set to 175 degrees C with a 140 g weight placed on top of the IC for approximately 5 min. The attached IC is also shown in Figure 4.

3.3.3. Measured read-range of the prototype RFID tag

To determine the read-range performance of the antenna design in the near-field of a UHF RFID reader at 920 MHz, 8 prototype tags were manufactured and tested. An Alien ALR-9650 EPC Class 1 Gen 2 scalable reader [7] with an integrated antenna was used to test the near-field performance of the tags. The reader antenna had a gain of 6 dBi and was circularly polarized (EIRP = 4.0 W). The measurement results for each tag are summarized in Table 6. A consistent near-field read-range can be observed showing that the antenna on the tag was performing appropriately with read-ranges comparable to a bar code system.

Finally, it should be mentioned that an additional benefit of this antenna design is the ability to achieve further read-ranges by improving the matching between the IC on the tag and the antenna; however since read-ranges comparable to bar code systems were desired for this work, the results in Table 6 are sufficient for the prototype tags with the antennas developed here with the reduced material.

CHAPTER 4. A LOW-COST FLEXIBLE PASSIVE UHF RFID TAG FOR SENSING MOISTURE BASED ON ANTENNA POLARIZATION

4.1. Introduction

A low-cost UHF RFID moisture sensor is designed on an inexpensive and flexible (Figure 6) paper substrate. Antenna polarization is used to sense the moisture.

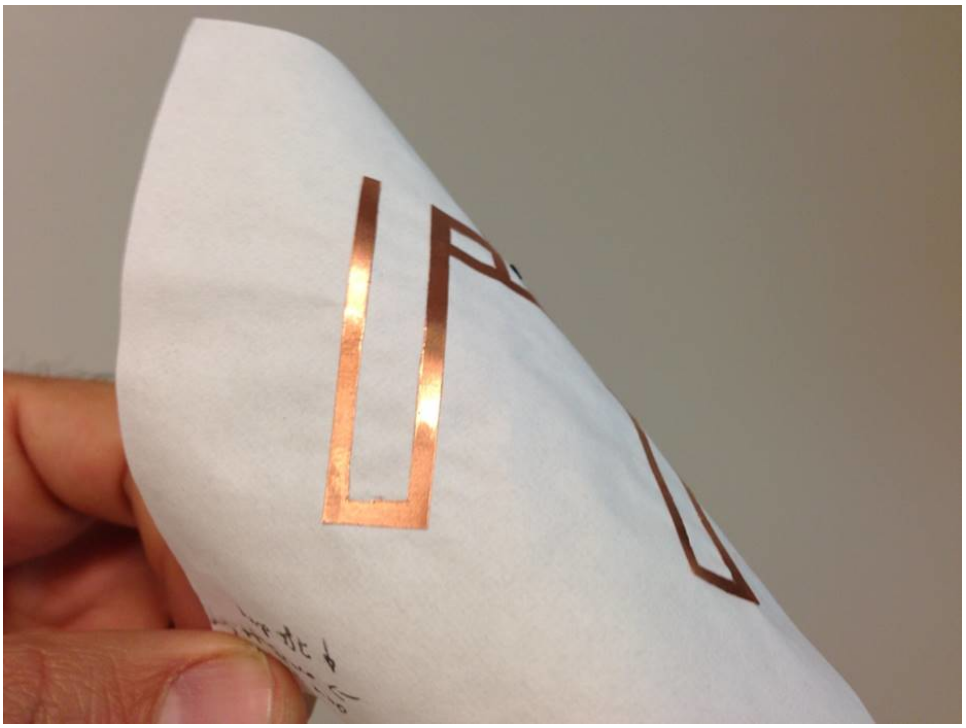

Figure 6. The flexibility of the fabricated antenna.

4.2. Functionality and Design

The dipole antenna is designed to sense the moisture from a certain reading distance at a certain transmitting power of the reader antenna. The reading distance depends on the moisture absorbed by the paper substrate when transmitting power of the reader antenna is fixed. Because good matching depends on the designed permittivity of the paper that is changed when it absorbs the moisture. That's why, based on the presence of moisture in the paper substrate, the dipole antenna is either

circularly polarized or linearly polarized. The RFID integrated circuit (IC) is used for power harvesting only.

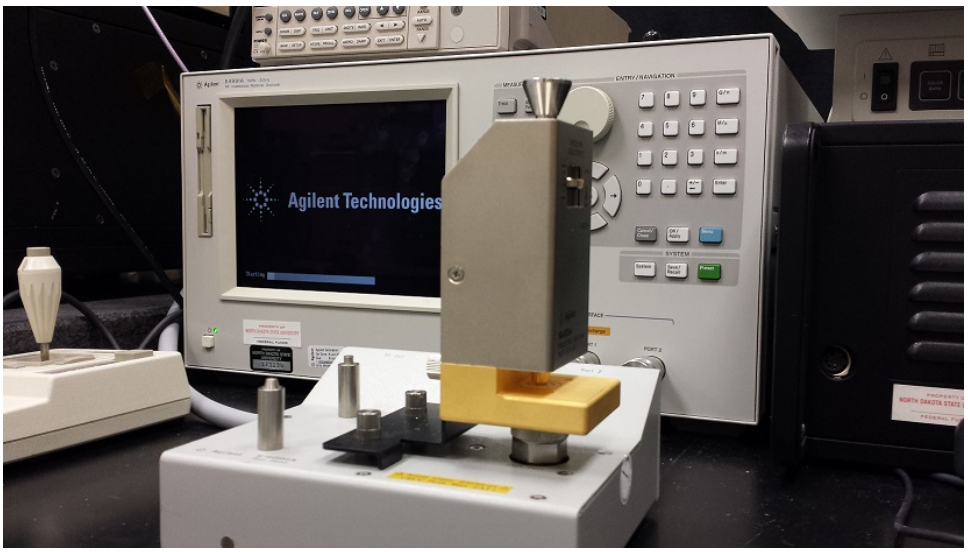

Figure 7. RF Impedance/Material Analyzer E4991A (1 MHz - 3 GHz).

4.2.1. Substrate selection

An inexpensive substrate Strathmore Marker 500 Series, acid-free, 100% cotton-based paper with thickness of 56 microns was used. The relative permittivity and loss tangent in different scenarios (dry and wet) were measured with the help of a RF Impedance/Material Analyzer E4991A (1 MHz - 3 GHz) (Figure 7) [35]. Five samples of the same paper substrate were tested and the average was used for the simulation. First we measured the dry paper, and the water was added to the paper to make it wet. Then we measured the wet paper. The average of relative permittivity and loss tangent of the paper substrate are shown in Table 7 and Table 8 for various values of moisture.

4.2.2. Antenna dimension

The antenna was designed having the dimensions of 47.35 mm $\times$ 43.8 mm on the paper substrate, and a minimum amount of copper was used to minimize the cost of the antenna. The antenna was designed as a dipole antenna with a 0.26 mm gap

between the two poles. Alien Higgs2 RFID IC was used in between the two poles which are responsible for power harvesting purposes. The dimensions of the antenna are shown in Figure 8.

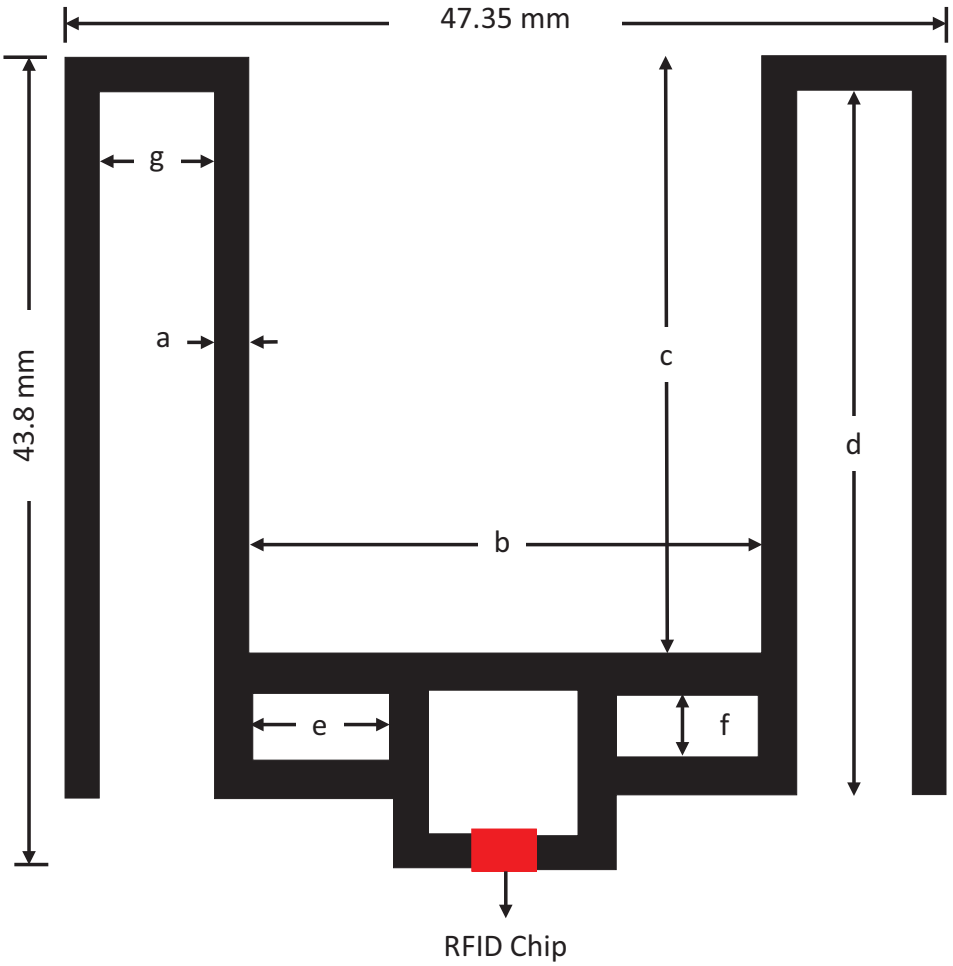

Figure 8. Dimension of the antenna; a= 2 mm, b = 27.35 mm, c = 32.35 mm, d = 38 mm, e = 7.6 mm, f = 3.65 mm, g = 6 mm.

Table 7. Average relative permittivity (ϵ_r) of the paper substrate.

State	Sample					
	1	2	3	4	5	Average
Dry	2.30	2.40	2.33	2.45	2.42	2.38
Wet	34.5	37.4	36.6	33.7	34.55	35.35

Table 8. Average loss tangent of the paper substrate.

State	Sample					
	1	2	3	4	5	Average
Dry	0.061	0.067	0.063	0.072	0.067	0.066
Wet	0.186	0.192	0.182	0.175	0.205	0.188

4.2.3. Fabrication

The antenna was manually cut from a 2-inch wide Cu tape using an Exacto knife under a microscope Leica S8 AP0[39]. The paper backing of the tape was then removed and the antenna was taped on the paper substrate. The Higgs2 IC was simply soldered to the leads.

Figure 9. Alien ALR-9610-BC RFID reader antenna.

4.2.4. Simulation results

The method of moments was used to simulate the antenna. The impedance of the Higgs2 IC depends on the operating frequency. The antenna was simulated to match the complex conjugate of IC impedance to achieve good matching at the desired resonant frequency. A linear sweep frequency from 800 MHz to 1.1 GHz was used. Based on the current distribution in simulation results the antenna was

circularly polarized when it is dry ($\epsilon_r = 2.38$, loss tangent = 0.066) (Figure 11). The antenna is linearly polarized when it is wet ($\epsilon_r = 35.35$, loss tangent = 0.188) (Figure 12).

Figure 10. Alien RFID reader.

4.2.5. Measurement results

The measurement can be done in two approaches. The read-range can be measured with a certain transmitting power of the reader antenna or the transmitting power can be measured with a certain read-range. In both approaches, the ratio of the horizontal to the vertical measurement (polarization ratio) will be the same. In this work, the first approach was explored. The read-ranges of five sample moisture sensors were measured in both the horizontal and vertical positions at different reading distances using the Alien ALR-9610-BC RFID reader antenna (at certain transmitting power) shown in Figure 9 and the Alien RFID reader[7] shown in Figure 10. The measurement results were matched with the expectation of the simulation results.

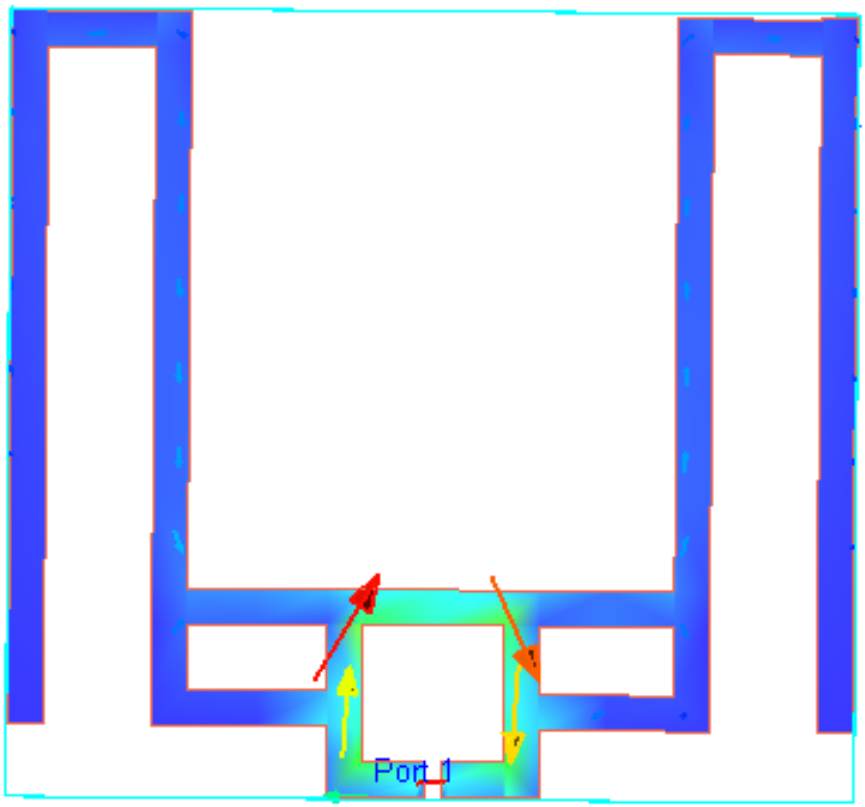

Figure 11. Current distribution when the relative permittivity $\epsilon_r = 2.38$ and the loss tangent = 0.066.

Based on the ratio of the horizontal reading distance to the vertical reading distance, the presence of the moisture in the paper can be sensed. All numbers in Tables 9 and 10 are reading distances in cm, except the ratios. Parallel ($\|$) means the reader antenna was parallel to the sensor and perpendicular ($\perp$) means the reader antenna was perpendicular to the sensor. Horizontal means the signal from the horizontally polarized reader antenna and vertical means signal from the vertically polarized reader antenna. Readings are consistent within a 40-degree deviation. deviation from the normal (i.e., 80-degree field of detection). The results are shown in the Tables 9 and Table 10 and it is shown that the perpendicular and parallel Horizontal/Vertical (H/V) ratio for the wet case is 2.7 and 4.4 times larger,

respectively, than the dry case. This change in the H/V ratio is caused by the moisture in the paper substrate and indicates that the sensor is working properly. As the paper used for this antenna is flexible and very thin, every sample was used only once for the sake of accurate measurement results.

4.3. Summary

Some noteworthy comments can be made based on the simulation results and the measurement results.

1. This sensor is the first low-cost moisture sensor which works based on the polarization.

2. As the antenna is fabricated on paper, it is very flexible compared to other solutions of low-cost moisture sensors.

3. The dimensions in Figure 8 are 47.35 mm × 43.8 mm ($0.144\lambda_0 \times 0.133\lambda_0$), which are comparatively smaller than the dimensions of other commercially available tags.

Table 9. Reading distance measurement when antenna is dry.

ID	Horizontal		Vertical		H/V Ratio	
	$\parallel$	$\perp$	$\parallel$	$\perp$	$\parallel$	$\perp$
8C99	549	549	213	183	2.57	3
6203	457	457	152	152	3	3
0BC4	549	549	183	183	3	3
35DF	594	594	305	274	1.95	2.17
9916	655	655	274	366	2.39	1.79
Average					2.58	2.59

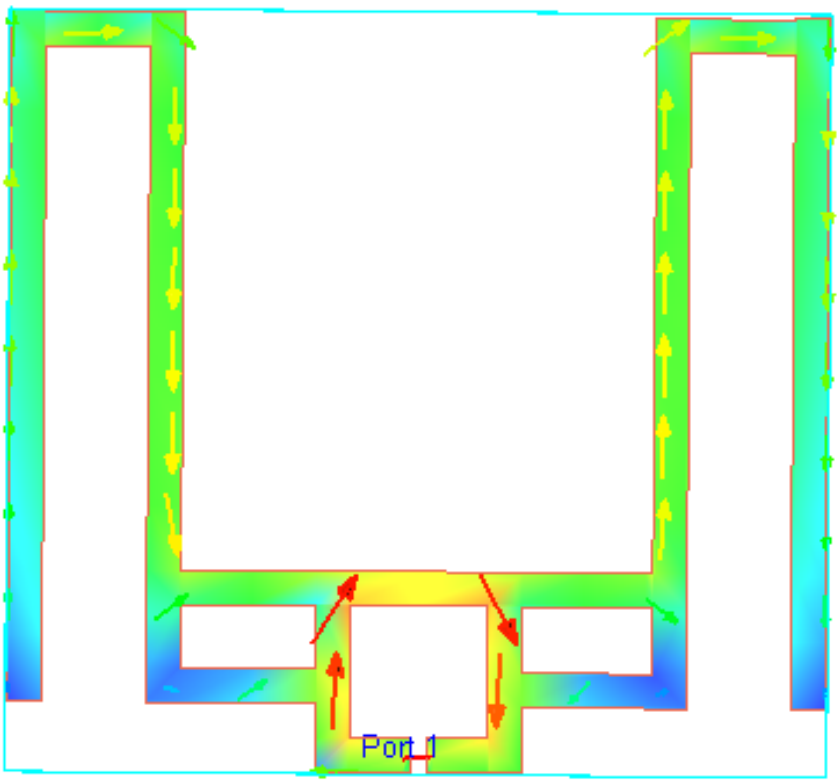

Figure 12. Current distribution when the relative permittivity $\epsilon_r = 35.35$ and the loss tangent = 0.188.

Table 10. Reading distance measurement when antenna is wet.

ID	Horizontal		Vertical		H/V Ratio	
	$\parallel$	$\perp$	$\parallel$	$\perp$	$\parallel$	$\perp$
8C99	549	549	61	76	9	7.2
6203	457	457	61	61	7.5	7.5
0BC4	549	549	30	91	18	6
35DF	518	518	46	61	11.33	8.5
9916	549	549	46	91	12	6
Average					11.57	7.04

CHAPTER 5. CONCLUSION

A reduced cost miniature antenna for near-field UHF radio frequency identification (RFID) applications has been presented. The antenna consisted of interconnected meander open complementary split ring resonator (MOCSRR) elements that were redesigned with 30% less conducting material. These new elements have been denoted as the R-MOCSRR elements where the R has been added to emphasize the reduced material benefits of the element. Furthermore, the R-MOCSRR based antenna was printed on a low-cost paper substrate, and the performance was measured. Overall, near-field read-ranges comparable to bar code systems were observed.

Moreover, a cost-effective solution has been investigated to sense moisture in an absorbing substrate using the polarization of a printed antenna on a passive RFID tag. In particular, a new antenna design with a polarization sensitive to the permittivity of the antenna substrate was presented. This sensitivity was then used to measure the moisture in a paper substrate, and it was shown that the polarization ratio of the sensor changed with moisture content. This makes this antenna design useful for sensing moisture without the requirement of a battery.

BIBLIOGRAPHY

[1] R. Weinstein,“ RFID: A technical overview and its application to the enterpise, ” *New Technology,* May - June 2005, pp. 27-33.

[2] K. Finkenzeller, *RFID Handbook:Fundamentals and Applications in Contactless Smart Cards and Identification,* John Wiley and Sons, West Sussex, England, 2003.

[3] X. Li and Z. Yang, “ Dual-printed-dipoles reader antenna for UHF near-field RFID applications, ” *IEEE Antennas Wireless Propag. Lett.,* vol. 10, 2011, pp. 239-242.

[4] X. Li and J. Liao, “ Eye-shaped segmented reader antenna for near-field UHF RFID applications, ” *Prog. in Electromag. Research,* vol. 114, 2011, pp. 481-493.

[5] X. Qing,C. K. Goh and Z. N. Chen, “ A broadband UHF near-field RFID antenna, ” *IEEE Trans. Antennas and Propag.,* vol. 58, no. 12, Dec. 2010, pp. 3829-3838.

[6] X. Qing, C. K. Goh and Z. N. Chen, “ Segmented loop antenna for UHF near-field RFID applications, ” *Electronics Lett.,* vol. 45, no. 17, Aug. 2009.

[7] Alien Technologies, [online], www.alientechnologies.com.

[8] J. Siden, A. Koptioug and M. Gulliksson, “ The smart diaper moisture detection system, ” *Microwave Symposium Digest, 2004 IEEE MTT-S International,* vol. 2, June 2004, pp. 659,662 Vol.2.

[9] L. Yambem, M. Yapici, and J. Zou, “ A new wireless sensor system for smart diapers, ” *Sensors Journal, IEEE,* vol. 8, no. 3, pp. 238,239, March 2008.

[10] M. SHERRON, “ Smart diaper, ” Sep. 23 2010, uS Patent App. 12/723,748. [Online]. Available: http://www.google.com/patents/US20100241094

[11] J. Clement, P. Secondo, and J. Tarte, “ Self-powered rfid tag activated by a fluid and method for using such rfid tags, ” May 8 2008, wO Patent App. PCT/EP2007/055,144. [Online]. Available: https://www.google.com/patents/WO2008052811A1?cl=en

[12] M. Amann, G. Striemer, F. Sherman, J. Joyce, J. BOURILKOV, M. Morrow, M. Franke, and S. SPECHT, “ Rfid transponder comprising sensor element, ” Jul. 4 2013, wO Patent App. PCT/US2012/070,274. [Online]. Available: https://www.google.com/patents/WO2013101539A1?cl=en

[13] S. Ahn, “ Defecation/urination detection system and method, ” Mar. 28 2013, uS Patent App. 13/701,609. [Online]. Available: https://www.google.com/patents/US20130076509

[14] P. De Haan and G. Van Heck, “ Moisture sensor, diaper with such a sensor, and method for detecting the presence and/or the intactness of the moisture sensor, ” May 20 2004, uS Patent App. 10/344,817. [Online]. Available: https://www.google.com/patents/US20040095247

[15] N. Kobayashi, “ Moisture sensor comprising conductive particles and a hygroscopic polymer of polyvinyl alcohol, ” May 16 2000, uS Patent 6,063,486. [Online]. Available: https://www.google.com/patents/US6063486

[16] W. R. Tinga, W. A. G. Voss, and D. F. Blossey, “ Generalized approach to multiphase dielectric mixture theory, ” *Journal of Applied Physics,* vol. 44, no. 9, 1973.

[17] Y. Sung, T. Jang, and Y. S. Kim, " A reconfigurable microstrip antenna for switchable polarization, " *Microwave and Wireless Components Letters, IEEE,* vol. 14, no. 11, pp. 534,536, Nov 2004.

[18] X. Qing and N. Yang, " A folded dipole antenna for rfid, " *Antennas and Propagation Society International Symposium, 2004. IEEE,* vol. 1, June 2004, pp. 97, 100 Vol.1.

[19] A. Toccafondi and P. Braconi, " Compact load-bars meander line antenna for uhf rfid transponder, " *Antennas and Propagation, 2006. EuCAP 2006. First European Conference on,* Nov 2006, pp. 1, 4.

[20] P. Nikitin, S. Lam, and K. V. S. Rao, " Low cost silver ink rfid tag antennas, " *Antennas and Propagation Society International Symposium, 2005 IEEE,* vol. 2B, July 2005, pp. 353,356 vol. 2B.

[21] R.-C. Hua and T.-G. Ma, " A printed dipole antenna for ultra high frequency (uhf) radio frequency identification (rfid) handheld reader, " *Antennas and Propagation, IEEE Transactions on,* vol. 55, no. 12, pp. 3742,3745, Dec 2007.

[22] S. Sajal, Y. Atanasov, O. Swenson, B. D. Braaten, and V. Marinov, " Simple and cost-efficient rfid tagging for hygiene applications, " *RISE Research, Innovation and Science for Engineered Fabrics Conference on,* Oct 2013.

[23] S. Sajal, Y. Atanasov, V. Marinov, O. Swenson, and B. D. Braaten, " Moisture sensor using the polarization of the dipole antenna, " *IMAPS NDSU Microelectronics Summit on,* Oct 2013.

[24] S.Sajal, Y. Atanasov, B. D. Braaten, V. Marinov and O. Swenson, " A Low Cost Flexible Passive UHF RFID Tag for Sensing Moisture Based on Antenna Po-

larization, " *IEEE International Conference on Electro/Information Technology,* Jun 2014,pp. 542-545.

[25] S. A. Weis, *RFID (Radio Frequency Identification): Principles and Applications*, www.eecs.harvard.edu,2007

[26] EPCglobal, [online], www.gs1.org

[27] ISO, [online], www.iso.org

[28] skyrfid, [online], www.skyrfid.com, last access date: 4th may'2014

[29] Marrocco, G., " The art of UHF RFID antenna design: impedance-matching and size-reduction techniques, " *Antennas and Propagation Magazine, IEEE ,* vol.50, no.1, pp.66,79, Feb. 2008 doi: 10.1109/MAP.2008.4494504

[30] Constantine A. Balanis, *Antenna Theory: Analysis and Design,* Harper and Row, Publishers, New York, 1982.

[31] A. Velez, F. Aznar, J. Bonache, M. C. Valazquez-Ahumada, J. Martel and F. Martin, " Open complementary split ring resonators (OCSRRs) and their application to wideband CPW band pass filter, " *IEEE Microw. Wireless Comp. Letters,* vol. 19, no. 4, pp. 197-199, Apr. 2009.

[32] B. D. Braaten and M. A. Aziz, " Using Meander Open Complementary Split Ring Resonator (MOCSRR) Particles to Design a Compact UHF RFID Tag Antenna, " *IEEE Antennas and Wireless Propagation Letters,* vol. 9, 2010, pp. 1037-1040.

[33] B. D. Braaten, " A Novel Compact UHF RFID Tag Antenna Designed with Series Connected Open Complementary Split Ring Resonator (OCSRR) Particles, " *IEEE Transactions on Antennas and Propagation,* vol. 58, no. 11, November, 2010, pp. 3728-3733.

[34] D. E. Anagnostou, A. A. Gheethan, A. Amert and K. W. Whites, " A Low-Cost WLAN "Green" PIFA Antenna on Eco- Friendly Paper Substrate, " *IEEE APS/URSI 2009 Intl Symp.,* Charleston, SC, USA, June 1-5, 2009.

[35] Advanced Design System-ADS 2009, Agilent Technologies, [online], www.agilent.com

[36] Speedline Technologies, [online], www.speedlinetech.com

[37] Henkel Corporation, [online], www.henkelna.com.

[38] Creative Materials Inc., [online], www.creativematerials.com.

[39] Leica Microsystems, [online], www.leica-microsystems.com

APPENDIX A. MATLAB CODE

The following

Impedance.m

The code was used to generate simulated input resistance and simulated input reactance of the prototype near-field UHF RFID Tags.

S11.m

The code was used to generate S11 values of the R-MOCSRR unit cell with the mesh removed simulated in Momentum and modeled using the equivalent circuit.

Higgs2.m

The code was used to find out the input impedance of the Higgs2 IC at particular frequency.

Higgs3.m

The code was used to find out the input impedance of the Higgs3 IC at particular frequency.

Impedance.m File

```
clc

clear all

Zin_infinity = [2.5-j*129 2.7-j*119 2.8-j*109 3.0-j*100 3.1-j*90 ...
    3.3-j*79.6 3.5-j*69 3.7-j*58 ...
     3.9-j*46.6 4.2-j*34.8 4.5-j*22.5 4.7-j*6.5 5.1+j*7 5.4+j*21.4 ...
        5.8+j*36.5 6.3+j*52];

Zin_1_1 = [14.3-j*129 15-j*120 15.8-j*111 16.6-j*102 17.5-j*93 ...
    18.4-j*83.4 19.5-j*73.5 20.6-j*63.3 ...
```

```
    21.9-j*52.7 23.3-j*41.7 24.8-j*30.3 26.5-j*18 28.4-j*5.8 ...
        30.5+j*7.3 32.8+j*21.3 35.5+j*36.2];

Zin_6_3 = [7.8-j*135 8.2-j*127 8.6-j*118 9.1-j*110 9.5-j*101 ...
   10.1-j*91 10.6-j*82 11.2-j*72 11.9-j*62, ...
    12.7-j*52 13.5-j*41 14.4-j*30.5 15.3-j*18.7 16.4-j*6.4 ...
        17.6-j*6.5 19+j*20.2];

Zin_6_9 = [17.8-j*126 18.7-j*117 19.6-j*108 20.7-j*98 21.8-j*89 ...
   23.1-j*79 24.4-j*69.4 25.9-j*59 ...
    27.6-j*48 29.4-j*36 31.4-j*25 33.6-j*12.8 36.1-j*.02 38.9+j*13.6 ...
        42+j*28 45.5+j*43.3];

f = 850:10:1000;

f_lines = [902 902 928 928];
lines = [-200 200 200 -200];
figure
subplot(2,1,1)
plot(f,real(Zin_infinity),'-',f,real(Zin_6_3),'d',f,real(Zin_1_1),
's',f,real(Zin_6_9),'o',f_lines,lines,'-')
xlabel('f (MHz)')
ylabel('Re(Z_{in}) (\Omega)')

axis([850 1000 0 50])

legend('\sigma = \infty','\sigma = 6.3x10^7 (S/m)','\sigma = ...
   1.12x10^7 (S/m)','\sigma = 6.99x10^6 (S/m)')
grid off


subplot(2,1,2)
```

```
plot(f,imag(Zin_infinity),'-',f,imag(Zin_6_3),'d',f,imag(Zin_1_1),
's',f,imag(Zin_6_9),'o',f_lines,lines,'-')
xlabel('f (MHz)')
ylabel('Im(Z_{in}) (\Omega)')
grid off

legend('\sigma = \infty','\sigma = 6.3x10^7 (S/m)','\sigma = ...
   1.12x10^7 (S/m)','\sigma = 6.99x10^6 (S/m)')
axis([850 1000 -150 150])
```

S11.m file

```
clc
clear all
S11_RMOCSRR_open = [.100    0.972
.150    0.941
.200    0.901
.250    0.855
.300    0.807
.350    0.759
.400    0.711
.450    0.665
.500    0.622
.550    0.581
.600    0.542
.650    0.506
.700    0.473
.750    0.441
.800    0.412
.850    0.384
.900    0.358
```

.950 0.333

1 0.309

1.05 0.287

1.1 0.265

1.15 0.244

1.2 0.224

1.25 0.204

1.3 0.185

1.35 0.166

1.4 0.148

1.45 0.13

1.5 0.112

1.55 0.095

1.6 0.078

1.65 0.062

1.7 0.048

1.75 0.039

1.8 0.038

1.85 0.048

1.9 0.063

1.95 0.081

2 0.101

2.05 0.123

2.1 0.145

2.15 0.169

2.2 0.193

2.25 0.219

2.3 0.245

2.35 0.271

2.4 0.298

2.45 0.322

2.5 0.344

```
2.55    0.356
2.6 0.344
2.65    0.237
2.7 0.871
2.75    0.849
2.8 0.799
2.85    0.803
2.9 0.825
2.95    0.853
3   0.88];

S11_RMOCSRR_filled=[.100    0.969
.150    0.933
.200    0.888
.250    0.839
.300    0.787
.350    0.735
.400    0.686
.450    0.638
.500    0.594
.550    0.552
.600    0.513
.650    0.477
.700    0.444
.750    0.413
.800    0.384
.850    0.356
.900    0.331
.950    0.306
1   0.283
1.05    0.261
1.1 0.24
```

1.15 0.22

1.2 0.201

1.25 0.182

1.3 0.164

1.35 0.146

1.4 0.128

1.45 0.112

1.5 0.095

1.55 0.079

1.6 0.065

1.65 0.052

1.7 0.043

1.75 0.04

1.8 0.046

1.85 0.057

1.9 0.072

1.95 0.089

2 0.107

2.05 0.126

2.1 0.146

2.15 0.166

2.2 0.187

2.25 0.209

2.3 0.23

2.35 0.251

2.4 0.271

2.45 0.287

2.5 0.296

2.55 0.283

2.6 0.194

2.65 0.836

2.7 0.443

```
2.75    0.793
2.8 0.719
2.85    0.721
2.9 0.741
2.95    0.767
3   0.797];

S11_RMOCSRR_mesh=[.100  0.971
.150    0.937
.200    0.895
.250    0.848
.300    0.798
.350    0.747
.400    0.698
.450    0.651
.500    0.607
.550    0.565
.600    0.526
.650    0.489
.700    0.455
.750    0.424
.800    0.394
.850    0.366
.900    0.339
.950    0.315
1   0.291
1.05    0.268
1.1 0.247
1.15    0.226
1.2 0.206
1.25    0.187
1.3 0.168
```

1.35 0.15

1.4 0.133

1.45 0.116

1.5 0.099

1.55 0.084

1.6 0.07

1.65 0.058

1.7 0.05

1.75 0.047

1.8 0.052

1.85 0.062

1.9 0.076

1.95 0.092

2 0.109

2.05 0.127

2.1 0.147

2.15 0.166

2.2 0.187

2.25 0.208

2.3 0.229

2.35 0.25

2.4 0.271

2.45 0.29

2.5 0.306

2.55 0.315

2.6 0.308

2.65 0.254

2.7 0.508

2.75 0.529

2.8 0.761

2.85 0.733

2.9 0.74

```
2.95    0.759
3   0.784];

s=0;
for L=1e-9:.25e-9:15e-9;
    for C = .1e-12:.5e-12:15e-12
        s=s+1;
f = 100e6:50e6:3e9;
w = 2*pi*f;

ZC = -j./(w*C);
ZL = j*w*L;
Zeq = ZC.*ZL./(ZC+ZL);
Z_0 = 50;

Z_in=Zeq*Z_0./(Zeq+Z_0);

gamma=(Z_in-Z_0)./(Z_in+Z_0);

S_11_ckt=20*log10(abs(gamma));

S_12_ckt=20*log10(abs(1+gamma));

diff=abs(S_11_ckt-20*log10(abs(S11_RMOCSRR_open(:,2))).');

diff_sum(s)=sum(diff);
if diff_sum(s)≤min(diff_sum)
    s_plot=s;
    L_eq=L;
    C_eq=C;
    S_11_ckt_plot=S_11_ckt
    S_12_ckt_plot=S_12_ckt;
```

```
else


end


    end
end


f1 = 915e6;
w = 2*pi*f1;
C = 1.6e-12;
L = 5.2e-9;
ZC = -j./(w*C);
ZL = j*w*L;
Zeq = ZC.*ZL./(ZC+ZL)


figure
plot(S11_RMOCSRR_open(:,1),20*log10(S11_RMOCSRR_open(:,2)),'s-',f/1e9,S_11_ckt_plot,'
xlabel('f (GHz)')
ylabel('|S_{11}| (dB)')
legend('Momentum','Equivalent Circuit')
```

Higgs2.m file

```
clear all;
r=1500;
c=1.2e-12;
f=860e6:1e6:960e6;
f1=915e6
Xc=1./(2.*j.*pi.*f.*c)
Z=(Xc.*r)./(r+Xc)
Imag=abs(imag(Z))
```

```
Real=real(Z)
figure;
[hAx,hLine1,hLine2]=plotyy(f/1e6,Real,f/1e6,Imag)
R=r/(1+4*pi*pi*f1*f1*c*c*r*r)
I=2*pi*f1*c*R*r
title('Frequency vs. IC Impedance')
xlabel('Frequency (MHz)')

ylabel(hAx(1),'Real |Z|') % left y-axis
ylabel(hAx(2),'Imag |Z|') % right y-axis
```

Higgs3.m file

```
clear all;
r=1500;
c=0.85e-12;
f=860e6:1e6:960e6;
f1=920e6
Xc=1./(2.*j.*pi.*f.*c)
Z=(Xc.*r)./(r+Xc)
Imag=abs(imag(Z))
Real=real(Z)
figure;
[hAx,hLine1,hLine2]=plotyy(f/1e6,Real,f/1e6,Imag)
R=r/(1+4*pi*pi*f1*f1*c*c*r*r)
I=2*pi*f1*c*R*r
title('Frequency vs. IC Impedance')
xlabel('Frequency (MHz)')

ylabel(hAx(1),'Real |Z|') % left y-axis
ylabel(hAx(2),'Imag |Z|') % right y-axis
```